ACS APPLIED MATERIALS & INTERFACES

Research Article

www.acsami.org

# SERS Detection and Removal of Mercury(II)/Silver(I) using Oligonucleotide-Functionalized Core/Shell Magnetic Silica Sphere@Au Nanoparticles

Min Liu, Zhuyuan Wang,* Shenfei Zong, Hui Chen, Dan Zhu, Lei Wu, Guohua Hu, and Yiping Cui*

Advanced Photonics Center, Southeast University, 2# Sipai Lou, Nanjing 210096, Jiangsu China

Supporting Information

**ABSTRACT:** Heavy metal ions, such as $Hg^{2+}$ and $Ag^{+}$, pose severe risks in human health and the environment. For sensitive detection and selective removal of $Hg^{2+}$ and $Ag^{+}$ ions, here, we demonstrate a surface-enhanced Raman scattering (SERS)-active platform by employing the oligonucleotide-functionalized magnetic silica sphere (MSS)@Au nanoparticles (NPs). This system exploits mismatched T−Hg−T and C−Ag−C bridges to capture $Hg^{2+}$ and $Ag^{+}$ ions, exhibiting excellent responses for $Hg^{2+}$ ions in the range of 0.1−1000 nM and for $Ag^{+}$ in the range of 10−1000 nM. The assay is highly selective for the target ions and does not respond to other metal ions. Additionally, the $Hg^{2+}$ and $Ag^{+}$ ions in this system can be effectively removed from surrounding solutions by an external magnetic field or through spontaneous precipitation. Moreover, more than 80% of the MSS@Au NPs can be easily recycled with the help of cysteine. We anticipate that the designed strategy could be extended to other analytes that can bind to DNA molecules with a high affinity, and can be used in many potential applications such as environmental renovation, toxin detection, and groundwater analysis.

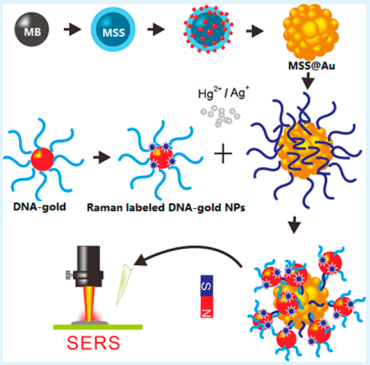


**KEYWORDS:** *surface-enhanced Raman scattering, heavy metal ions, magnetic silica nanospheres, T−Hg−T bridges*

## INTRODUCTION

Heavy metal contaminations have been one of the most challenging problems throughout the world for many decades. In particular, the water-soluble mercuric (II) ion ($Hg^{2+}$) is generally considered to be one of the most toxic forms of heavy metal,[1−4] because of its bonding nature to thiol groups in proteins[2] and its accumulative properties in the ecosystem. It can cause kidney/liver failure, bone softening, neurological disorder (for example, Minamata disease), immune damage, and other ill effects,[1−4] which are extremely hazardous to human health. Another heavy metal ion, $Ag^{+}$, is extremely toxic to bacteria, phytoplankton, and invertebrates.[5,6] In previous studies, it has been demonstrated that $Ag^{+}$ ions can elicit deformities and even cause death of embryos once introduced into the body excessively.[7] Therefore, sensitive detection and selective removal of $Hg^{2+}$ and/or $Ag^{+}$ ions are of paramount importance in the assessment of contamination risks, as well as in the elimination of potential health hazards. Currently, multiple sensors[8−11] based on different signal transduction mechanisms have been developed to detect these ions, including electrochemical,[12] colorimetric,[13] surface Plasmon resonance[14] and fluorescent sensors.[15−17] In particular, researchers have put a spotlight on the fluorescent and colorimetric approaches owing to their high sensitivity, fast response and easy operation. For example, Wu et al. created a QD-DNA-Au NP ensemble by utilizing the nanometal surface energy transfer (NSET) mechanism,[15] which exhibited a LOD of 0.4 and 1.2 ppb to $Hg^{2+}$ in the buffer solution and in river water, respectively. Very recently, this research group fabricated a highly sensitive and selective GO-based fluorescent sensor,[17] which realized label-free $Hg^{2+}$ ions detection for the first time. Additionally, Jung et al. reported a series of nanomaterials for detecting and removing toxic metal ions, which can recognize target ions with high degrees of selectivity among heavy metal ions in aqueous solution, including acyclic receptor immobilized MS,[18] BODIPY-functionalized MSN[19] and so on.[20−23] Usually, there is more than one type of ions in pollutant, and thus the ability to detect and remove multiple ions is critical for many practical applications, such as environmental renovation, toxin monitoring, and groundwater analysis. To date, it still remains a great challenge to develop a method for sensitive detection and selective removal of multiple ions simultaneously.

Surface-enhanced Raman scattering (SERS)[24−31] is a technique that allows vibrational modes of individual bond to be probed optically and is rich in spectral information. Previously, Kim et al. exploited a single nanowire-on-film (SNOF) SERS sensor[32] for detecting $Hg^{2+}$ ions based on thymine−thymine mismatch pairs (T−Hg−T). Similarly, Liu et al. have detected $Hg^{2+}$ ions using gold nanoparticles/graphene heterojunctions as SERS sensors.[33] Among them, assembling SERS-active gold nanoparticles into well-defined hot SERS nanostructures has offered a great benefit to the sensitive

Received: February 7, 2014
Accepted: April 16, 2014
Published: April 16, 2014

   dx.doi.org/10.1021/am5006282 | ACS Appl. Mater. Interfaces 2014, 6, 7371−7379

detection. Recently, oligonucleotide-functionalized magnetic silica sphere (MSS)@Au core/shell nanoparticles (NPs) has emerged as one of the most efficient and widely used configurations in SERS-related studies owing to their unique combinational properties,[34−39] such as controlled particle size, tunable surface plasmon resonance (SPR), high chemical stability, as well as high biocompatibility. More importantly, these nanoparticles can be easily captured, aggregated and removed by a magnet, which provide a convenient platform for the sensitive detection and selective removal of heavy metal ions.[21,22] To date, as far as we know, there has been no report about SERS-based detection and magnetic removal of multiple toxic metal ions, simultaneously.

Here, we report a strategy that combines oligonucleotide-modified MSS@Au core/shell NPs and SERS technique to simultaneously detect and remove $Hg^{2+}$/$Ag^{+}$ ions with a high sensitivity and selectivity. The concept behind this approach is illustrated in Scheme 1. In our proposed approach, two types of

**Scheme 1. Schematic Illustration of the SERS-Active System for $Hg^{2+}$/$Ag^{+}$ Ion Detection Based on T−Hg−T/C−Ag−C Bridges Using DNA-Au NPs and DNA-MSS@Au NPs**

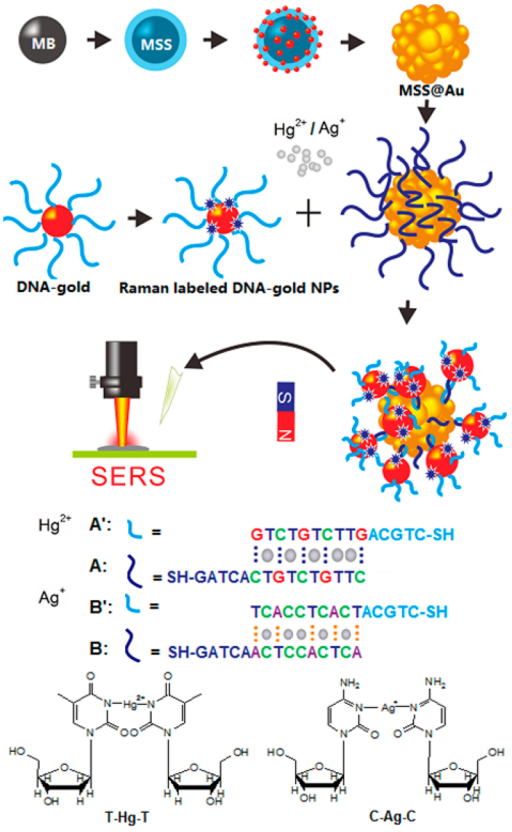


oligonucleotide (ssDNA) with different capture segments are functionalized to the MSS@Au NPs and the Raman reporter-labeled gold NPs,[40] respectively. The capture segments in the two sequences are complementary except for five T (or C) sites. The base-pair binding energy between the capture segments is not sufficient to hybridize them fully. But T−T mismatched base pairs can effectively capture $Hg^{2+}$ ions to form T−Hg−T bridges and C−C mismatched base pair can exclusively recognize $Ag^{+}$ ions to form C−Ag−C bridges, enabling the capture segments to hybridize fully, and thus generating plasmonic hotspots to enhance the SERS signals[4,12,32,33,41] of Raman reporters. This SERS-active platform exhibits several distinctive advantages that are not available from conventional metal sensing systems. First of all, it allows to detect $Hg^{2+}$ and $Ag^{+}$ ions simultaneously with high sensitivity and selectivity. The sensitivity of 0.1 nM for $Hg^{2+}$ ion is ∼10 times more sensitive than conventional optical $Hg^{2+}$ sensors, and about 2 orders of magnitude lower than U.S.A. EPA-defined maximum contaminant level (MCL) in drinking water (No EPA-defined MCL of $Ag^{+}$ ions). In addition, this SERS-active nanosystem, owing to its magnetic property, can be applied for the removal of $Hg^{2+}$ and $Ag^{+}$ ions, indicating a great potential in environmental applications. Moreover, the MSS@Au NPs are recyclable, which enormously facilitates the experiments and makes the defined protocol a low-cost technique. This technique will provide a promising alternative way for chemical and environmental monitoring of metallic species.

## EXPERIMENTAL SECTION

**Materials.** $FeCl_3·6H_2O$, $FeCl_2·4H_2O$, $AgNO_3$, $HAuCl_4·4H_2O$, polyvinyl-pyrrolidone(PVP), (3-aminopropyl) trimethoxysilane (APTMS), and sodium citrate were purchased from Alfa Aesar (Tianjin) Chemical Reagent Co. Ltd. (Beijing, China). NaOH, HCl, NaCl, $HAuCl_4·4H_2O$, KCl, $CuCl_2$, $NH_4Cl$, $CaCl_2$, $CoCl_2$, $CdCl_2$, $Zn(NO_3)_2$, $Cr(NO_3)_3$, tetrakis(hydroxymethyl) phosphonium chloride (THPC), agarose, and poly(allylamine hydrochloride) (PAH) were purchased from Sinopharm Chemical Reagent Co. Ltd. (Beijing, China). Mercuric nitrate ($Hg(NO_3)_2$) was purchased from Xiya Reagent Co. Ltd. (Chengdu, China). All of the DNA sequences, as shown in Table S1 in the Supporting Information, were custom synthesized by Sangon Co. Ltd. (Shanghai, China) and purified by HPLC. All the reagents were used as received. Deionized water with a resistivity of 18.2 MΩ was obtained from a Millipore water purification system.

**Preparation of MSS@Au NPs.** MSS NPs were prepared as previously reported.[35] First, for fabricating 100 nm magnetic beads, 1.350 g of $FeCl_3·6H_2O$, 3.85 g of $NH_4Ac$, and 0.4 g of sodium citrate were dissolved in 70 mL of ethylene glycol. The mixture was stirred vigorously for 1 h at 160 °C under the protection of nitrogen, and then transferred into a Teflon-lined stainless-steel autoclave. The autoclave was heated at 200 °C for 17 h, and then cooled to room temperature. The resulting magnetic beads were washed 3 times with ethanol and 2 times with water. Then, for silica coating, 40 μL of the prepared magnetic beads solution and 1 mL of PAH (40 mg/mL) were dissolved in 3.6 mL of deionized water. The mixture was sonicated for 1 h and washed twice with water before being dissolved in 10 mL (50 mg/mL) of PVP. The solution was sonicated for 30 min, and shaken overnight. Subsequently, these magnetic beads were separated by a magnet, and washed twice with water and ethanol, respectively. The resulting nanoparticles were dissolved in 10 mL of ethanol, and then 1 mL of ammonia (26−28% ammonia) and 20−30 μL of TEOS were injected. The mixture was sonicated for 8 h and washed 4 times with ethanol. After the magnetic collection, these magnetic silica spheres were dissolved in 10 mL of ethanol. Then, a mixture of 200 μL of APTMS and 100 μL of water was injected. The solution was shaken overnight, and then heated to 65 °C. These amine-functionalized MSS NPs were separated by a magnet, followed by being washed 2 additional times with water, and finally stored in 0.4 mL of deionized water.

For the preparation of MSS@Au NPs, a seed-mediated protocol[36] was used. First, the bare gold seeds were synthesized by reacting 2 mL of $HAuCl_4·4H_2O$ (1%) and 12 μL of THPC in 50 mL of NaOH (10 mM). The solution was stirred until the color changed to black. To this solution was added dropwise 0.4 mL of prepared MSS NPs. The mixture was shaken overnight, and then washed twice with water. The resulting nanoparticles were separated by a magnet and stored in 0.4 mL of deionized water before use. Subsequently, the growth solution was prepared by dissolving 12.5 mg of $K_2CO_3$ in 150 μL of $HAuCl_4$·


dx.doi.org/10.1021/am5006282 | ACS Appl. Mater. Interfaces 2014, 6, 7371−7379

$4H_2O$ (1%) and 50 mL of water. The solution was stirred until the color changed from pale yellow to clear colorless. Then, 20 μL of prepared MSS@Au seeds was mixed with 50 mL of the growth solution and 100 μL of formaldehyde solution (30−40%). Finally, the mixture was sonicated for 5 min, during which the color of the solution changed to azure blue. This color change suggested that the MSS@Au NPs were successfully synthesized.

**DNA Functionalization of MSS@Au NPs.** The DNA functionalization of MSS@Au NPs was accomplished following a previously published protocol.[35] Typically, 0.1 mL of thiol-terminated DNA sequences (20 μM) was added to 0.9 mL of prepared MSS@Au NPs (1 nM), and incubated for 12 h at room temperature, followed by 30 s sonication. Then, a mixture with a final concentration of 0.01% SDS, 10 mM PBS buffer (pH 7.4) and 0.05 M sodium were added, and the resultant mixture was shaken overnight. Four additional aliquots of sodium chloride were added over a period of 8 h to achieve a final sodium chloride concentration of 0.3 M. Sonication was performed for 30 s between additions, followed by the incubation of 12 h. The DNA-MSS@Au NPs were washed 3 times with water and stored in 0.3 M sodium chloride/10 mM PBS buffer (pH 7.4).

**Synthesis of Raman Reporter-Labeled DNA-gold NPs.** Raman reporter-labeled DNA-gold NPs were prepared according to a previously published protocol.[40,42] For the synthesis of ∼15 nm gold nanoparticles, 2 mL of $HAuCl_4{\cdot}4H_2O$ was dissolved in 200 mL of deionized water. The mixture was heated to boiling, and 8 mL of sodium citrate (1%) was quickly injected to the solution with a vigorously stirring. The resulting mixture was allowed to react for 15 min, during which its color turned to wine-red. The resulting nanoparticles were purified from unreacted materials by three rounds of centrifugation, and redispersed in deionized water. For DNA functionalization, 0.9 mL of the prepared gold nanoparticles (1 μM) was mixed with 0.1 mL of thiol-terminated DNA (200 μM). Then, a solution with a final concentration of 0.01% SDS, 10 mM PBS buffer (pH 7.4) and 0.05 M sodium were added, and the mixture was shaken for 12 h. Four additional aliquots of sodium chloride were added over a period of 8 h to achieve a final sodium chloride concentration of 0.3 M, followed by overnight incubation at room temperature. The excess DNA was removed by repeated centrifugation (30 min at 10000 × g). Then, 3 μL of Raman reporter (10 mM, DTNB or 4-MBA) was dissolved in 1 mL of the prepared DNA-gold NP solutions and shaken overnight. Finally, the Raman reporter-labeled DNA-gold NPs were purified by washing twice with water, and stored in 0.3 M sodium chloride/PBS buffer (pH 7.4).

**Determination of $Hg^{2+}$or/and $Ag^{+}$ Ions.** For detection of $Hg^{2+}$ or $Ag^{+}$ ions, 0.5 mL of the as-prepared DNA-MSS@Au NPs solution was mixed with the Raman-labeled DNA-gold solution, and 0.1 mL of $Hg^{2+}$ or $Ag^{+}$ ions solution at a series of different concentrations. In the mixture, the final concentration ratio of DNA-MSS@Au NPs:DNA-gold NPs was set to 10 nM:1 μM (see the Supporting Information). Similarly, for simultaneous detection of both ions, 0.5 mL of DNA-MSS@Au solution was mixed with the DNA-gold solution containing two types of Raman-labeled DNA gold NPs, follow by adding 0.1 mL of $Hg^{2+}$ and $Ag^{+}$ ions solution at a series of different concentrations. The final concentration of each type of DNA-gold NPs was set to 0.8 μM. And the final concentration of DNA-MSS@Au was adjusted to 10 nM. The mixture was heated to 70 °C for 30 min, and then shaken for 4 h on an orbital shaker at room temperature, during which mixtures were sonicated for 2 min every 30 min. Then the samples were washed twice with PBS (pH 7.4) and water, respectively, and separated by a magnet and stored in PBS buffer for SERS measurement. After SERS measurements, the DNA-MSS@Au NPs can be recycled with the help of cysteine for further rounds of detection. In detail, the sediment that contains DNA-MSS@Au NPs and Raman reporter-labeled DNA-gold NPs, was redispersed in 1 mL of PBS. The excessive cysteine was added for capturing $Hg^{2+}$ or $Ag^{+}$ in the T−Hg−T or C−Ag−C bridges. After that, the mixture was incubated on an orbital shaker for 4 h, and the DNA-MSS@Au NPs were finally collected by a magnet or through spontaneous precipitation, and stored in PBS for further use.

**Instrumentation and Measurement.** Optical absorption spectra of samples were collected using a Shimadzu UV-3600 PC spectrophotometer (Shimadzu, Kyoto, Japan) with quartz cuvettes of 1 cm path length. Transmission electron microscope (TEM) images were obtained with a FEI Tecnai $G^2$ T20 electron microscope (FEI, Hillsboro, OR, USA) operating at 200 kV. Zeta potential measurements were conducted on a Zeta Potential analyzer (ZEN3690, Malvern, UK) from Malvern Inc. Laser beam at 633 nm was irradiated to measure the electrophoretic mobility of particles using the principles of dynamic light scattering. 1% agarose gel electrophoresis was performed using a mini-sub cell GT system (Bio-Rad, USA) and visualized by a Gel Imaging System (Tanon, China). SERS measurements were performed using a Raman spectroscopy (HORIBA, France) with a 100× objective (NA = 0.9). He−Ne laser with 632.8 nm radiation was used for excitation, and the laser power at the sample position was 2.3 mW. The acquisition time of all SERS spectra was 30 s.

## RESULTS AND DISCUSSION

**Characterization of Nanoparticles.** Figure 1 shows the TEM images of the nanoparticles at various stages in the synthesis process. As shown, the magnetic beads (MBs) with an average diameter of 140 nm display a well-defined spherical or spherical-like structure. As described before, these MBs were coated with a silica shell whose thickness is about 15−20 nm (Figure 1b). Subsequently, the resulting nanoparticles were functionalized with APTMS that displaces the surfactant and allows for the attachment of 3−5 nm gold nanoparticles to MSS

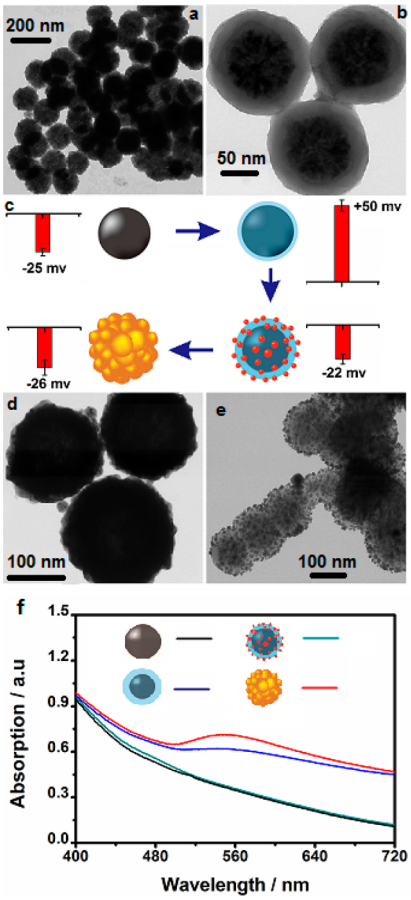


**Figure 1.** Characterizations of the nanoparticles at various stages of the synthesis process, including the TEM images of (a) MB, (b) MSS, (e) MSS@Au seeds, and (d) MSS@Au core/shell nanoparticles; (c) zeta potential of these nanoparticles, as well as (f) the absorption spectra of these nanoparticles.


dx.doi.org/10.1021/am5006282 | ACS Appl. Mater. Interfaces 2014, 6, 7371−7379

surfaces. In this step, the zeta potential of the MSS NPs increased to +50 mV, as shown in Figure 1c. This zeta potential change confirmed that the amine functionalization has been performed successfully. After that, 3−5 nm Au seeds were adsorbed on the surfaces of MSS NPs by electrostatic forces (Figure 1e), and these Au seeds acted as nucleation sites to form a continuous gold shell by reducing $HAuCl_4$. Figure 1d shows the representative TEM image of the as-prepared MSS@Au core/shell NPs, in which a well-defined spherical morphology can be observed. These MSS@Au NPs are typically 100−110 nm in radii, which was determined by measuring 200 nanoparticles in TEM images (see Figure S2 in the Supporting Information).

To further confirm the formation of MSS@Au nanostructure, the absorption spectra of nanoparticles at each stage of synthesis process were measured (Figure 1f). As shown, the MBs display a strong absorption edge in the wavelength region of 400 nm. After coating silica shell, no obvious difference in the absorption spectrum is observed, since silica is almost optically transparent in the range of 400−800 nm. Importantly, the adsorption of 3−5 nm Au seeds onto the MSS surfaces brings a broad absorption band near ∼530 nm. After the final reduction step, this feature band shifts to ∼532 nm with an increased intensity, indicating that Au is present as a shell on the MSS surfaces. Together, the absorption results of nanoparticles are fully consistent with the proposed synthetic pathway illustrated in Scheme 1, which further confirmed the formation of MSS@Au NPs.

**Determination of $Hg^{2+}$ Ions.** For $Hg^{2+}$ ions detection, the freshly prepared MSS@Au NPs were functionalized with the T-rich DNA sequences (sequences A) according to Scheme 1. Correspondingly, the gold nanoparticles (see Figure S3 in the Supporting Information) were functionalized with the partially complementary sequences (sequences A′) to specifically recognize $Hg^{2+}$ ions. Here, five mismatched T−T base pairs[4,32] were designed for the ligation of $Hg^{2+}$ ions, with five intervening matched C-G base pairs for enhancing the affinity between sequences A and A′, as well as for avoiding the self-folding of the single stranded DNA. The DNA functionalization was confirmed by zeta potential results (see Table S2 in the Supporting Information). Moreover, to produce a SERS signal, in this case, DTNB[43] was labeled on the DNA-gold NP surfaces as the Raman reporter.

The formation of SERS platforms was confirmed by 1% agarose gel electrophoresis (see Figure S4 in the Supporting Information). As indicated in the figure, the DNA−gold NPs (lane 1) in gel were moved toward the anode without difficulty at the driving voltage. Nevertheless, the migration of DNA-MSS@Au NPs (lane 2) was powerfully retarded by the cross-linking of the agarose gel due to their big sizes. For the same reason, the migration of the complexes (SERS platforms) containing both nanoparticles was also strongly prevented (lane 3). In contrast, a new retarded band is observed (lane 4−6) in the presence of cysteine due to the separation of the DNA-gold NPs from complexes (the cysteine can capture the $Hg^{2+}$ ions from the T−Hg−T bridges and ultimately result in the dehybridization of the double stranded DNA, which will be discussed later). Compared with lane 4−6, no retarded band is observed in lane 3, implying that the formation of complex was indeed a result of DNA hybridization rather than the nonspecific adsorption.

Figure 2a presents the typical SERS spectra of these SERS-active systems under different $Hg^{2+}$ concentrations. As shown,

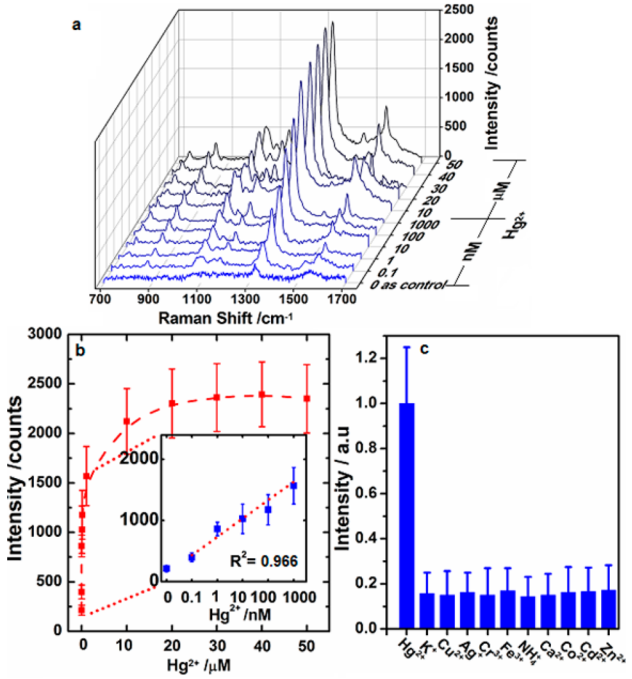


**Figure 2.** (a) SERS spectra under different concentration of $Hg^{2+}$ ions. (b) Plot of 1333 $cm^{-1}$ band intensities versus the concentration of $Hg^{2+}$ ions. The inset shows a dynamic range and linearly fitted line. (c) Selectivity testing of the SERS-active platform. Millimolar concentrations of various metal ions, including $K^+$, $Cu^{2+}$, $Ag^+$, $Cr^{3+}$, $Fe^{3+}$, $NH^+$, $Ca^{2+}$, $Co^{2+}$, $Cd^{2+}$, and $Zn^{2+}$, shows far weaker SERS responses than $Hg^{2+}$ ions at nanomolar level. The data of b and c were obtained from five measurements and the error bars represent standard deviation.

in the absence of $Hg^{2+}$ions, no obvious SERS peak is observed aside from a very weak one at 1333 $cm^{-1}$, possibly due to the nonspecific adsorption. In the presence of $Hg^{2+}$ ions, the most pronounced SERS bands of DTNB at 1333, 1067, 1152, and 1558 $cm^{-1}$ are unambiguously observed, indicating that $Hg^{2+}$ ions stabilized the mismatched T−T pairs and brought the DTNB-labeled gold NPs to the MSS@Au surfaces. In addition, the SERS intensity increases as a function of $Hg^{2+}$ ion concentration, revealing that more DTNB-labeled DNA-gold nanoparticles were captured by MSS@Au NPs via T−Hg−T bridges with the increase in $Hg^{2+}$ ions.

The increasing trend of SERS intensity with $Hg^{2+}$ concentration was further summarized in Figure 2b. Here, the intense SERS peak at 1333 $cm^{-1}$ in the spectra has been used as a calibration band. As shown, a distinct increase in SERS intensity is observed as the $Hg^{2+}$ concentration increases from 0.1 to 1000 nM. Above 1000 nM, saturation in signal intensity is observed, indicating the maximum response concentration. A calibration curve in the concentration range from 0.1 to 1000 nM is shown in the inset of Figure 2b. The linear equation is determined as $y = 300\log x + 730$ $(1000 > x > 0.1)$ with the correlation coefficient $R^2 = 0.966$, where $y$ is the SERS intensity and $x$ is the concentration of $Hg^{2+}$ ion. Note that the aggregation of nanoparticles will form nanojunctions between two plasmonic surfaces, which would generate additional SERS "hotspots" and thus lead to an abnormally high level of SERS signals. To minimize the influence of aggregation to SERS signals, the amount of DNA bound to each gold NP was rigidly controlled to less than 20/particle. As a result, the DNA-gold NPs will get less opportunity of connecting more than one of


dx.doi.org/10.1021/am5006282 | ACS Appl. Mater. Interfaces 2014, 6, 7371−7379

MSS@Au NP, minimizing the aggregation of nanoparticles and the fluctuations of SERS signals (see Figure S5 in the Supporting Information). Here, an acceptable sample-to-sample and batch-to-batch variation was obtained by measuring three separate batches of 15 samples (see Figure S6 and Table S3 in the Supporting Information), revealing relatively good reproducibility of this SERS-based detection strategy.

To develop a specific assay capable of $Hg^{2+}$ ions detection, the SERS response to other potential contaminants must be minimized. To establish the specificity, SERS responses of this approach to other metal ions were investigated and the results are shown in Figure 2c. As expected, even millimolar concentrations of typical metal ions, including $K^+$, $Cu^{2+}$, $Ag^+$, $Cr^{3+}$, $Fe^{3+}$, $NH_4^+$, $Ca^{2+}$, $Co^{2+}$, $Cd^{2+}$, and $Zn^{2+}$, exhibit much weaker responses than $Hg^{2+}$ at nM level. Additionally, the ability of this SERS system to detect $Hg^{2+}$ ions in complex solution was also investigated. When interrogated with a complex solution containing multiple ionic species, including $Na^+$, $Ag^+$, $Zn^{2+}$, and $Cu^{2+}$, the SERS regime was able to detect $Hg^{2+}$ without interference (data not shown), making this assay a potential alternative method for $Hg^{2+}$ ion detection.

**Determination of $Ag^+$ Ions.** For $Ag^+$ ions detection, 4-MBA was chosen as Raman reporter to produce SERS signals.[42,43] Figure 3a shows the SERS spectra under different concentration of $Ag^+$ ions. As shown, in the absence of $Ag^+$ ions, two very weak bands at 1080 and 1582 $cm^{-1}$ are present, indicating that there existed some nonspecific binding between DNA-gold NPs and MSS@Au NPs. In the presence of $Ag^+$ ions, the typical SERS peaks of 4-MBA at 1080, 1180, 1390, and 1582 $cm^{-1}$ can be clearly observed, implying that the $Ag^+$ ions stabilized the C−C mismatched base pairs and brought the 4-MBA-labeled gold NPs to the MSS@Au surfaces. As the concentration of $Ag^+$ increases, the SERS signal becomes intensified, indicating the further formation of C−Ag−C bridges. An accurate investigation of the $Ag^+$ ions influence on SERS intensity was performed by tracking the intensity of SERS peak at 1080 $cm^{-1}$, as shown in Figure 3b. It is observed that the SERS intensity increases significantly in the $Ag^+$ concentration range from 10 nM to 1 $\mu$M, and reaches a saturation value with $Ag^+$ concentration above 1 $\mu$M. The linear equation is determined as $y = 574\log x - 152x - 152$ ($x > 10$) with the correlation coefficient $R^2 = 0.963$, as shown in the inset of Figure 3b. The present limit of detection (LOD) was estimated to be 10 nM. The LOD of $Ag^+$ is approximately 2 orders of magnitude higher than that of $Hg^{2+}$, probably resulting from the weaker interaction between C−Ag−C in comparison with T−Hg−T.

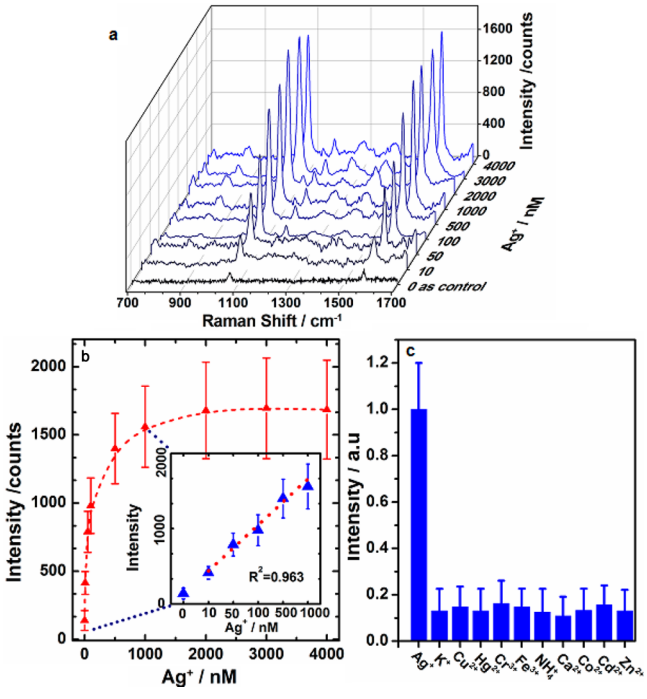


**Figure 3.** (a) SERS spectra under different $Ag^+$ ions concentration. (b) Plot of 1080 $cm^{-1}$ band intensities versus the concentration of $Ag^+$ ions. The inset shows a dynamic range and linearly fitted line. (c) Selectivity testing of the SERS-active platform. Millimolar concentrations of various metal ions, including $K^+$, $Cu^{2+}$, $Hg^{2+}$, $Cr^{3+}$, $Fe^{3+}$, $NH^+$, $Ca^{2+}$, $Co^{2+}$, $Cd^{2+}$, and $Zn^{2+}$, shows far weaker SERS responses than $Ag^{2+}$ at micromolar level. The data of b and c were obtained from five measurements and the error bars represent standard deviation.

Furthermore, the selectivity of this nanosystem for $Ag^+$ ions was investigated. As illustrated in Figure 3c, the separate addition of each kind of ion including $K^+$, $Cu^{2+}$, $Hg^{2+}$, $Cr^{3+}$, $Fe^{3+}$, $NH_4^+$, $Ca^{2+}$, $Co^{2+}$, $Cd^{2+}$, and $Zn^{2+}$ into the aqueous samples (~millimolar) did not result in an obvious SERS signal at 1080 $cm^{-1}$, whereas $Ag^+$ ions at concentration of ~$\mu$M level have caused a very intense SERS intensity, demonstrating the high selectivity of the SERS-active system for $Ag^+$ ions. The system's ability to detect $Ag^+$ ions in complex solutions ($Na^+$, $Hg^{2+}$, $Zn^{2+}$, and $Cu^{2+}$) was also investigated, and the result demonstrated that it was able to detect $Ag^+$ without interference (data not shown).

**Simultaneous Detection of $Hg^{2+}$ and $Ag^+$ Ions.** We have investigated the ability of this system to simultaneously detect $Hg^{2+}$ and $Ag^+$ ions. The principle of simultaneous detection is schematically illustrated in Figure 4a. The MSS@Au NPs are first functionalized with a 25 bases DNA sequence (sequence AB). In the presence of $Hg^{2+}$ and $Ag^+$ ions, the different segments in sequence AB can simultaneously capture $Hg^{2+}$ and $Ag^+$ ions by forming T−Hg−T and C−Ag−C bridges with the DNA sequences A′′ and B′′. As evidenced by the TEM micrograph presented in Figure S7 in the Supporting Information, some DNA-gold NPs were captured by MSS@Au NPs, indicating that this strategy is applicable in simultaneous detection of both ions. According to the scheme, the $Ag^+$ and $Hg^{2+}$ ions may be considered as inputs for the activation of an "OR" logic gate operation. Here, the state of no intense SERS peak is defined as a "False" output, as shown in Figure 4b. In the absence of $Hg^{2+}$ and $Ag^+$ ions, only very weak SERS signals are observed, corresponding to an input (0,0) and an output '0'. In the presence of $Hg^{2+}$ or $Ag^+$ ions, input (0, 1) or (1, 0), one or two intense SERS peaks are observed, corresponding to an output '1'. In the presence of both $Hg^{2+}$ and $Ag^+$, three intense SERS bands are observed, giving rise to an output '1'.

Moreover, the detailed dependence of SERS signal intensity on the concentration ratio of the two components is presented in Figure 4c (The full range data is shown in Figure S8 in the Supporting Information). For a straightforwardly visual representation, the SERS spectra are displayed in a color-contrast spectral barcode,[44] wherein the lines, the color contrast and the line width represent the Raman peaks, the relative intensity and the width of the peaks, respectively. As shown, in the absence of $Hg^{2+}$ and $Ag^+$ ions, the SERS barcode presents very weak azure lines around 1080, 1333, and 1582 $cm^{-1}$, which arise from nonspecific adsorption as mentioned before. As the


dx.doi.org/10.1021/am5006282 | ACS Appl. Mater. Interfaces 2014, 6, 7371−7379

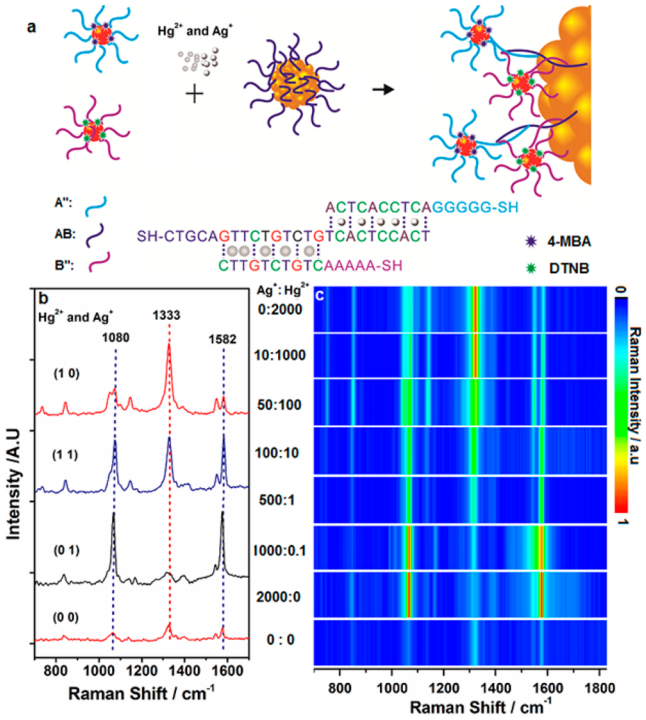


**Figure 4.** (a) Schematic illustration of simultaneous detection of $Hg^{2+}$ and $Ag^{+}$ ions. (b) SERS output of "OR" logical gate as different ($Hg^{2+}$, $Ag^{+}$) inputs. (c) SERS barcodes obtained at a variety of $C_{Ag^{+}}$:$C_{Hg^{2+}}$ from 0:2000 to 0:0.

concentration ratio of $Hg^{2+}$ to $Ag^{+}$ decreases from 2000:0 to 0:2000, the color of the lines at 1080 and 1582 $cm^{-1}$ changed from red to azure gradually. Simultaneously, the color of line at 1333 $cm^{-1}$ changed from azure to red simultaneously. The dynamic ranges for $Hg^{2+}$ and $Ag^{+}$ ions in simultaneous detection were summarized in Figure 5. As shown, SERS signals exhibit excellent responses for $Hg^{2+}$ions in the range of 0.1−1000 nM and for $Ag^{+}$ ions in the range of 50−1000 nM. The linear equations are determined as $y = 289\log x+726$ ($x > 0.1$, $R^2=0.968$) for $Hg^{2+}$ ions and $y = 631\log x -770$ ($x > 50$, $R^2 = 0.978$) for $Ag^{+}$ ions, respectively. The LOD for $Ag^{+}$ ions is

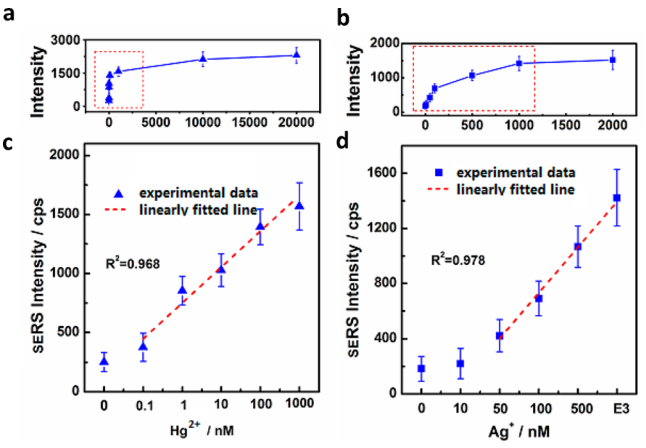


**Figure 5.** (a) Plot of 1333 $cm^{-1}$ band intensities versus the concentration of $Hg^{2+}$ions and (b) plot of 1080 $cm^{-1}$ band intensities versus the concentration of $Ag^{+}$ ions in simultaneous detection of both ions. (c, d) Dynamic range (red box in a, b) and linearly fitted line. The error bars represent standard deviation from five measurements.

slightly higher than that in single ion detections. This is because the DNA sequences connecting the MSS@Au NPs and DNA-Au NPs contains 25 bases (Figure 4a), which is longer than those used in single ion detections. In contrast with most of previously reported approaches, this SERS assay displays a higher sensitivity and a wider the dynamic ranges (see Table 1). Above all, these results strongly demonstrate that the defined SERS-active system can be successfully utilized to simultaneously detect $Hg^{2+}$ and $Ag^{+}$ ions.

**Removal of $Hg^{2+}$ and $Ag^{+}$ Ions from Surrounding Solutions.** This system is also designed to remove $Hg^{2+}$ and $Ag^{+}$ ions from surrounding solutions, as illustrated in Figure 6a. In the experiments, Raman reporter-labeled gold NPs and MSS@Au NPs were incubated with a PBS buffer that contains $Hg^{2+}$ or $Ag^{+}$ (1 $\mu$M) ions for 2 h. Afterward, an external magnet was applied to magnetically retain the sedimentation. In contrast to the solution without adding $Hg^{2+}$ ions, the $Hg^{2+}$ ions solution shows a significant decrease in turbidity after applying an external magnet (photographs in Figure 6a), suggesting that $Hg^{2+}$ ions have been successfully isolated from the solution. Interestingly, these nanoparticles can also settle down spontaneously by gravity after standing for 5 days at room temperature, implying a great potential in environmental applications. Similar phenomena were also observed in $Ag^{+}$ ions removing. To evaluate the removal efficiency, the supernatant concentration of $Hg^{2+}$/$Ag^{+}$ ions was monitored and the results are shown in Figure 6b. Starting with 1 $\mu$M, the concentration of $Hg^{2+}$ ions were decreased to ∼2 nM after the magnetic removal or spontaneous precipitation, which is also confirmed by atomic fluorescence spectrometry (AFS, Figure S9 in the Supporting Information). Similarly, the supernatant $Ag^{+}$ concentration were decreased to below ∼10 nM from 1 $\mu$M after the removal steps. It should be noted that the removal efficiency could be improved by repeating the removal steps in practical applications.

Another advantage of this system is the ability to recycle the MSS@Au NPs. In the recycle experiments, cysteine were added to the mixtures for capturing the $Hg^{2+}$/$Ag^{+}$ ions from the T−Hg−T/C−Ag−C bridges, which ultimately resulted in the dehybridization of the double stranded DNA, as schematically illustrated in Figure 6c. In a typical experiment, about ∼30% of MSS@Au NPs were allowed to be recollected after 5 rounds of recycles, which means that the maximum remained amount of recyclable MSS@Au NPs was ∼80% each time (see Figure S10 in the Supporting Information), whereas ∼20% of MSS@Au NPs was lost during the magnetic collection and the extensive washing steps.

Finally, the performance of recycled MSS@Au NP has been investigated by UV−vis spectroscopy, SERS spectroscopy, zeta potential measurements, and TEM. For comparison, the concentrations of MSS@Au NPs before and after recycling were adjusted to a constants value. As shown in Figure S11 in the Supporting Information, no significant differences are observed in the normalized UV−vis spectra as well as in TEM images, suggesting that the structures and the compositions of MSS@Au NPs remained unchanged after 5 rounds of recycling. However, the Zeta potential of the recycled MSS@NPs slightly increased from −50 mV to −43 mV, and the SERS signals decreased ∼28% from before recycling. Based on Zeta potential and SERS data, we calculated that ∼3.9% of DNA bound to the MSS@Au NPs has been washed away from nanoparticles' surfaces after each round of recycling, which may slightly affect the reproducibility in practical applications.

**Table 1. Comparison of Assay Method for Monitoring Heavy Metal Ions**

| target ions | detection transduction method | linear range | LOD | ref |
|---|---|---|---|---|
| Hg(II)/Ag(I) | SERS | 0.1−1000 nM/10−1000 nM | 0.1 nM/1 nM | our results |
| Hg(II) | fluorescence (D-ODN-F sensor) | 40−100 nM | 40 nM | ref16 |
| Hg(II) | fluorescence (NSET sensor) | 2−60 nM | 2 nM | ref15 |
| Hg(II) | fluorescence (GO-based fluorescent sensor) | 1−50 nM | 0.92 nM | ref17 |
| Hg(II) | colorimetric detection | 1−10 $\mu$M | 1 $\mu$M | ref13 |
| Hg(II) | SERS | 1pM~1 $\mu$M | 1 pM | ref31 |
| Pb(II)/Ag(I) /Hg(II) | charge-transfer resistance | 10 pM~10 $\mu$M/100−800 nM/10 $\mu$M~0.1 nM | 10 pM/10 nM/0.1 nM | ref12 |
| Hg(II) | SERS | 10pM~100 nM | 10 pM | ref32 |
| Hg(II) | fluorescence (turn on) | 10−8000 nm | 2.6 nm | ref8 |
| Hg(II) | ICP-MS | a | 4.0 nM | ref10 |
| Hg(II) | colorimetric and fluorimetric detection | 10 $\mu$M~0.1 nM | 10 $\mu$M | ref20 |
| Pb(II) /Hg(II) | fluorescence | 128−1000 nM/121−1000 nM | 128 nM/121 nM | ref11 |

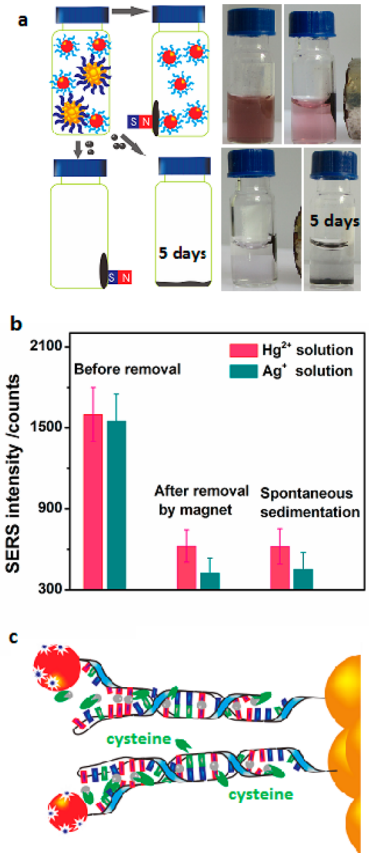


**Figure 6.** (a) Schematic illustration of the $Hg^{2+}/Ag^{+}$ ions removal by a magnet or through spontaneous sedimentation, and the corresponding photographs. (b) Total efficiency of removal was calculated by measuring the SERS intensity of collected sediments. (c) Schematic illustration of dsDNA dehybridization with the help of cysteine.

## CONCLUSION

In summary, we have demonstrated a SERS-active nanoplatform for sensitive detection and selective removal of $Hg^{2+}$ or $Ag^{+}$ ions based on the T−Hg−T and C−Ag−C mismatched base pairs. The concentration-dependent SERS signals exhibited an excellent response for $Hg^{2+}$ in the range of 0.1−1000 nM and for $Ag^{+}$ in the range of 10−1000 nM. Besides, in this SERS platforms, $Hg^{2+}$ or $Ag^{+}$ ions can be conveniently removed from the surrounding solutions by a magnet or though spontaneous precipitation. The residual $Hg^{2+}$ ions can be decreased to ~2 nM and the residual $Ag^{+}$ ions can be decreased to ~10 nM after removing operations. Moreover, 80% of the MSS@Au NPs can be easily recycled with the help of cysteine each time. This SERS-active platform exhibits several distinctive advantages that are not available from conventional metal sensing systems. First of all, it allows to detect $Hg^{2+}$ and $Ag^{+}$ ions simultaneously with high sensitivities. Second, this system can be used for the removal of $Hg^{2+}$ and $Ag^{+}$ ions, indicating a great potential in environmental applications. Finally, the MSS@Au NPs are recyclable, which facilitates the experiments and makes the defined protocol a low−cost technique. We envision that the demonstrated strategy could be extended to many other analytes that can bind to DNA molecules with a high affinity, which could potentially be used in other applications such as groundwater analysis and toxin detection.

## ASSOCIATED CONTENT

### Supporting Information

Determination of the optimal concentrations of the MSSA@Au and DNA-Au NPs in SERS detection; sizes of MSS@Au NPs; TEM and absorption of gold NPs; 1% agarose gel electrophoresis result; TEM images of nanoparticles on the state of aggregation and dispersion; sample-to-sample and batch-to-batch reproducibility in $Hg^{2+}$ ions detection; TEM images of nanomaterial in the presence of both ions; SERS spectra at variety of concentration ratio $C_{Ag^{+}}$:$C_{Hg^{2+}}$; determination of Hg(II) concentration before and after removing step by using AFS; recycling of MSS@Au NPs; performances of MSS@Au NPs before and after recycling; table containing DNA sequences; zeta potential of prepared nanoparticles; table listing sample-to-sample and batch-to-batch SERS signals variation in $Hg^{2+}$ ions detection. This material is available free of charge via the Internet at http://pubs.acs.org.

## AUTHOR INFORMATION

### Corresponding Authors

*E-mail: cyp@seu.edu.cn.
*E-mail: wangzy@seu.edu.cn.

### Notes

The authors declare no competing financial interest.

## ACKNOWLEDGMENTS

This work was supported by the Natural Science Foundation of China (NSFC) (61275182, 61177033, 21104009), Science Foundation for The Excellent Youth Scholars of Southeast University, the Scientific Research Foundation of Graduate School of Southeast University (YBJJ1125), the Scientific Innovation Research Foundation of College Graduate in

Jiangsu Province (CXZZ12_0094), and the Fundamental Research Funds for the Central Universities.

## REFERENCES


(1) Cho, E. S.; Kim, J.; Tejerina, B.; Hermans, T. M.; Jiang, H.; Nakanishi, H.; Yu, M.; Patashinski, A. Z.; Glotzer, S. C.; Stellacci, F.; Grzybowski, B. A. Ultrasensitive Detection of Toxic Cations through Changes in the Tunnelling Current across Films of Striped Nanoparticles. *Nat. Mater.* **2012**, *11*, 978−985.

(2) Omichinski, J. G. Toward Methylmercury Bioremediation. *Science* **2007**, *317*, 205−206.

(3) Hoang, C. V.; Oyama, M.; Saito, O.; Aono, M.; Nagao, T. Monitoring the Presence of Ionic Mercury in Environmental Water by Plasmon-Enhanced Infrared Spectroscopy. *Sci. Rep.* **2013**, *3*, 1175 DOI: 10.1038/srep01175.

(4) Long, F.; Zhu, A.; Shi, H.; Wang, H.; Liu, J. Rapid on-Site/in-Situ Detection of Heavy Metal Ions in Environmental Water Using a Structure-Switching DNA Optical Biosensor *Sci. Rep.* **2013**, *3*. DOI: 10.1038/srep02308.

(5) Yuan, X.; Setyawati, M. I.; Tan, A. S.; Ong, C. N.; Leong, D. T.; Xie, J. Highly Luminescent Silver Nanoclusters with Tunable Emissions: Cyclic Reduction-Decomposition Synthesis and Antimicrobial Properties. *NPG Asia Mater.* **2013**, *5*, e39 DOI: 10.1038/am.2013.3.

(6) Croteau, M.-N.; Misra, S. K.; Luoma, S. N.; Valsami-Jones, E. Silver Bioaccumulation Dynamics in a Freshwater Invertebrate after Aqueous and Dietary Exposures to Nanosized and Ionic Ag. *Environ. Sci. Technol.* **2011**, *45*, 6600−6607.

(7) Lee, K. J.; Nallathamby, P. D.; Browning, L. M.; Osgood, C. J.; Xu, X.-H. N. In Vivo Imaging of Transport and Biocompatibility of Single Silver Nanoparticles in Early Development of Zebrafish Embryos. *ACS Nano* **2007**, *1*, 133−143.

(8) Deng, L.; Ouyang, X.; Jin, J.; Ma, C.; Jiang, Y.; Zheng, J.; Li, J.; Li, Y.; Tan, W.; Yang, R. Exploiting the Higher Specificity of Silver Amalgamation: Selective Detection of Mercury(II) by Forming Ag/Hg Amalgam. *Anal. Chem.* **2013**, *85*, 8594−8600.

(9) Li, M.; Gou, H.; Al-Ogaidi, I.; Wu, N. Nanostructured Sensors for Detection of Heavy Metals: A Review. *ACS Sustainable Chem. Eng.* **2013**, *1*, 713−723.

(10) Rodrigues, J. L.; Torres, D. P.; de Oliveira Souza, V. C.; Batista, B. L.; de Souza, S. S.; Curtius, A. J.; Barbosa, F., Jr Determination of Total and Inorganic Mercury in Whole Blood by Cold Vapor Inductively Coupled Plasma Mass Spectrometry (Cv Icp-Ms) with Alkaline Sample Preparation. *J. Anal. Atom. Spectrosc.* **2009**, *24*, 1414−1420.

(11) Chung, C. H.; Kim, J. H.; Jung, J.; Chung, B. H. Nuclease-Resistant DNA Aptamer on Gold Nanoparticles for the Simultaneous Detection of $Pb^{2+}$ and $Hg^{2+}$ in Human Serum. *Biosens. Bioelectron.* **2013**, *41*, 827−832.

(12) Lin, Z.; Li, X.; Kraatz, H.-B. Impedimetric Immobilized DNA-Based Sensor for Simultaneous Detection of $Pb^{2+}$, $Ag^{+}$, and $Hg^{2+}$. *Anal. Chem.* **2011**, *83*, 6896−6901.

(13) Xue, X.; Wang, F.; Liu, X. One-Step, Room Temperature, Colorimetric Detection of Mercury ($Hg^{2+}$) Using DNA/Nanoparticle Conjugates. *J. Am. Chem. Soc.* **2008**, *130*, 3244−3245.

(14) Wang, G.; Lim, C.; Chen, L.; Chon, H.; Choo, J.; Hong, J.; deMello, A. Surface-Enhanced Raman Scattering in Nanoliter Droplets: Towards High-Sensitivity Detection of Mercury (II) Ions. *Anal. Bioanal. Chem.* **2009**, *394*, 1827−1832.

(15) Li, M.; Wang, Q.; Shi, X.; Hornak, L. A.; Wu, N. Detection of Mercury(II) by Quantum Dot/DNA/Gold Nanoparticle Ensemble Based Nanosensor Via Nanometal Surface Energy Transfer. *Anal. Chem.* **2011**, *83*, 7061−7065.

(16) Ono, A.; Togashi, H. Highly Selective Oligonucleotide-Based Sensor for Mercury(II) in Aqueous Solutions. *Angew. Chem., Int. Ed.* **2004**, *43*, 4300−4302.

(17) Li, M.; Zhou, X.; Ding, W.; Guo, S.; Wu, N. Fluorescent Aptamer-Functionalized Graphene Oxide Biosensor for Label-Free Detection of Mercury(II). *Biosens. Bioelectron.* **2013**, *41*, 889−893.

(18) Kim, E.; Eun Kim, H.; Jin Lee, S.; Sung Lee, S.; Lyong Seo, M.; Hwa Jung, J. Reversible Solid Optical Sensor Based on Acyclic-Type Receptor Immobilized Sba-15 for the Highly Selective Detection and Separation of Hg(II) Ion in Aqueous Media. *Chem. Commun.* **2008**, 3921−3923.

(19) Lee, H. Y.; Bae, D. R.; Park, J. C.; Song, H.; Han, W. S.; Jung, J. H. A Selective Fluoroionophore Based on Bodipy-Functionalized Magnetic Silica Nanoparticles: Removal of $Pb^{2+}$ from Human Blood. *Angew. Chem., Int. Ed.* **2009**, *121*, 1265−1269.

(20) Kim, E.; Seo, S.; Seo, M. L.; Jung, J. H. Functionalized Monolayers on Mesoporous Silica and on Titania Nanoparticles for Mercuric Sensing. *Analyst.* **2010**, *135*, 149−156.

(21) Lee, M. H.; Wu, J.-S.; Lee, J. W.; Jung, J. H.; Kim, J. S. Highly Sensitive and Selective Chemosensor for $Hg^{2+}$ Based on the Rhodamine Fluorophore. *Org. Lett.* **2007**, *9*, 2501−2504.

(22) Park, M.; Seo, S.; Lee, I. S.; Jung, J. H. Ultraefficient Separation and Sensing of Mercury and Methylmercury Ions in Drinking Water by Using Aminonaphthalimide-Functionalized $Fe_3O_4$@$SiO_2$ Core/Shell Magnetic Nanoparticles. *Chem. Commun.* **2010**, *46*, 4478−4480.

(23) Lee, S. J.; Lee, J. E.; Seo, J.; Jeong, I. Y.; Lee, S. S.; Jung, J. H. Optical Sensor Based on Nanomaterial for the Selective Detection of Toxic Metal Ions. *Funct. Mater.* **2007**, *17*, 3441−3446.

(24) Aikens, C. M.; Madison, L. R.; Schatz, G. C. Raman Spectroscopy: The Effect of Field Gradient on Sers Aikens, C. M.; Madison, L. R.; Schatz, G. C. Raman Spectroscopy: The Effect of Field Gradient on SERS. *Nat. Photonics* **2013**, *7*, 508−510.

(25) Cheng, I. F.; Chang, H.-C.; Chen, T.-Y.; Hu, C.; Yang, F.-L. Rapid (<5[Emsp14]Min) Identification of Pathogen in Human Blood by Electrokinetic Concentration and Surface-Enhanced Raman Spectroscopy. *Sci. Rep.* **2013**, *3*, 2365 DOI: 10.1038/srep02365.

(26) Lim, D.-K.; Jeon, K.-S.; Kim, H. M.; Nam, J.-M.; Suh, Y. D. Nanogap-Engineerable Raman-Active Nanodumbbells for Single-Molecule Detection. *Nat. Mater.* **2010**, *9*, 60−67.

(27) Kim, K.; Han, H. S.; Choi, I.; Lee, C.; Hong, S.; Suh, S.-H.; Lee, L. P.; Kang, T. Interfacial Liquid-State Surface-Enhanced Raman Spectroscopy. *Nat. Commun.* **2013**, *4*, 2182 DOI: 10.1038/ncomms3182.

(28) Ayas, S.; Cinar, G.; Ozkan, A. D.; Soran, Z.; Ekiz, O.; Kocaay, D.; Tomak, A.; Toren, P.; Kaya, Y.; Tunc, I.; Zareie, H.; Tekinay, T.; Tekinay, A. B.; Guler, M. O.; Dana, A. Label-Free Nanometer-Resolution Imaging of Biological Architectures through Surface Enhanced Raman Scattering. *Sci. Rep.* **2013**, *3*, 2624 DOI: 10.1038/srep02624.

(29) Hodges, M. D.; Kelly, J. G.; Bentley, A. J.; Fogarty, S.; Patel, I. I.; Martin, F. L.; Fullwood, N. J. Combining Immunolabeling and Surface-Enhanced Raman Spectroscopy on Cell Membranes. *ACS Nano* **2011**, *5*, 9535−9541.

(30) Nie, S.; Emory, S. R. Probing Single Molecules and Single Nanoparticles by Surface-Enhanced Raman Scattering. *Science* **1997**, *275*, 1102−1106.

(31) Zhang, L.; Chang, H.; Hirata, A.; Wu, H.; Xue, Q.-K.; Chen, M. Nanoporous Gold Based Optical Sensor for Sub-Ppt Detection of Mercury Ions. *ACS Nano* **2013**, *7*, 4595−4600.

(32) Kang, T.; Yoo, S. M.; Yoon, I.; Lee, S.; Choo, J.; Lee, S. Y.; Kim, B. Au Nanowire-on-Film SERS Sensor for Ultrasensitive $Hg^{2+}$ Detection. *Chem.—Eur. J.* **2011**, *17*, 2211−2214.

(33) Ding, X.; Kong, L.; Wang, J.; Fang, F.; Li, D.; Liu, J. Highly Sensitive Sers Detection of $Hg^{2+}$ Ions in Aqueous Media Using Gold Nanoparticles/Graphene Heterojunctions. *ACS Appl. Mater. Interfaces* **2013**, *5*, 7072−7078.

(34) Cutler, J. I.; Auyeung, E.; Mirkin, C. A. Spherical Nucleic Acids. *J. Am. Chem. Soc.* **2012**, *134*, 1376−1391.

(35) Li, J.-M.; Ma, W.-F.; You, L.-J.; Guo, J.; Hu, J.; Wang, C.-C. Highly Sensitive Detection of Target Ssdna Based on Sers Liquid Chip Using Suspended Magnetic Nanospheres as Capturing Substrates. *Langmuir* **2013**, *29*, 6147−6155.

(36) Park, H. H.; Woo, K.; Ahn, J.-P. Core−Shell Bimetallic Nanoparticles Robustly Fixed on the Outermost Surface of Magnetic Silica Microspheres. *Sci. Rep.* **2013**, *3*, 1497 DOI: 10.1038/srep01497.

(37) Onses, M. S.; Pathak, P.; Liu, C.-C.; Cerrina, F.; Nealey, P. F. Localization of Multiple DNA Sequences on Nanopatterns. *ACS Nano* **2011**, *5*, 7899−7909.
(38) Kim, J.-H.; Chung, H.-W.; Lee, T. R. Preparation and Characterization of Palladium Shells with Gold and Silica Cores. *Chem. Mater.* **2006**, *18*, 4115−4120.
(39) Behra, M.; Azzouz, N.; Schmidt, S.; Volodkin, D. V.; Mosca, S.; Chanana, M.; Seeberger, P. H.; Hartmann, L. Magnetic Porous Sugar-Functionalized Peg Microgels for Efficient Isolation and Removal of Bacteria from Solution. *Biomacromolecules* **2013**, *14*, 1927−1935.
(40) Lee, K.; Drachev, V. P.; Irudayaraj, J. DNA−Gold Nanoparticle Reversible Networks Grown on Cell Surface Marker Sites: Application in Diagnostics. *ACS Nano* **2011**, *5*, 2109−2117.
(41) Feng, D.-Q.; Liu, G.; Zheng, W.; Liu, J.; Chen, T.; Li, D. A Highly Selective and Sensitive on-Off Sensor for Silver Ions and Cysteine by Light Scattering Technique of DNA-Functionalized Gold Nanoparticles. *Chem.Commun.* **2011**, *47*, 8557−8559.
(42) Liu, M.; Wang, Z.; Zong, S.; Zhang, R.; Zhu, D.; Xu, S.; Wang, C.; Cui, Y. SERS-Based DNA Detection in Aqueous Solutions Using Oligonucleotide-Modified Ag Nanoprisms and Gold Nanoparticles. *Anal. Bioanal. Chem.* **2013**, *405*, 6131−6136.
(43) Wang, Z.; Zong, S.; Li, W.; Wang, C.; Xu, S.; Chen, H.; Cui, Y. SERS-Fluorescence Joint Spectral Encoding Using Organic−Metal−Qd Hybrid Nanoparticles with a Huge Encoding Capacity for High-Throughput Biodetection: Putting Theory into Practice. *J. Am. Chem. Soc.* **2012**, *134*, 2993−3000.
(44) Xu, J.; Turner, J. W.; Idso, M.; Biryukov, S. V.; Rognstad, L.; Gong, H.; Trainer, V. L.; Wells, M. L.; Strom, M. S.; Yu, Q. In Situ Strain-Level Detection and Identification of Vibrio Parahaemolyticus Using Surface-Enhanced Raman Spectroscopy. *Anal. Chem.* **2013**, *85*, 2630−2637.